Composites Communications 38 (2023) 101523

Contents lists available at ScienceDirect

Composites Communications

journal homepage: www.elsevier.com/locate/coco

Tailorable activation of thermoresponsive composite structures incorporating wavy heaters via hybrid manufacturing

Yuan-Fang Zhang [a,*], Honggeng Li [b], Chengyun Long [a], Yi Xiong [c], Qi Ge [b,**]

[a] Shien-Ming Wu School of Intelligent Engineering, South China University of Technology, Guangzhou, 511442, PR China
[b] Department of Mechanical and Energy Engineering, Southern University of Science and Technology, 1088 Xueyuan Avenue, Shenzhen, 518055, PR China
[c] School of System Design and Intelligent Manufacturing, Southern University of Science and Technology, 1088 Xueyuan Avenue, Shenzhen, 518055, PR China

ARTICLE INFO

Keywords:
Joule-heating
Tailorable activation of smart materials
Shape-memory polymers
Thermoresponsive composite structures

ABSTRACT

The activation method of thermoresponsive materials greatly affects the practical use of smart structures composed thereof. Despite extensive research that relies on methods using high ambient temperatures or planar heaters, the efficient and tailorable activation of relatively thick thermoresponsive composite structures remains challenging. Herein, we present a concept of embedding a wavy heater into a thermoresponsive material matrix to form a composite structure with parametrically designed thermal activation behavior, through a facile manufacturing approach combining 3D-printing and laser-cutting. We develop a numerical model to predict the transient heat transfer for varying wavy shapes of heater, and experimentally validate the numerical results. The exploration of the design space using the numerical model shows a reduction of up to 82% in heating time using the wavy design compared with the flat design. Finally, we demonstrate experimentally the stiffness tuning in thermoresponsive composite structures. This work paves the way for large-scale thermoresponsive composite structures with applications in aerospace and architecture.

1. Introduction

Thermoresponsive smart materials that change physical properties upon thermal stimuli are widely used in various engineering settings [1–13]. Many efforts have been made with focus on the thermal activation of relatively thin structures made of such materials [1,8,10,13–15]. However, when it comes to practical applications, large-scale structures made of thermoresponsive materials are often used because of their enhanced mechanical performances [11,16–22]. The thermal activation of such structures becomes lengthier and less uniform as the thickness increases. Conventional activation methods commonly involve heating with a high ambient temperature [11,22,23], relying on the heat convection which is slow and sometimes infeasible. Recent works have suggested heating methods with embedded Joule-heating elements, but usually with a planar layout [4,10,14,17,19,24–29]. The heat source is often concentrated in the mid-plane or on one side of the structure, thus restricting the spatial distribution of heat generation across the volume of the smart material composite.

In this work, we propose a concept of embedding a wavy heater into a thermoresponsive material matrix to form a composite structure whose thermal activation behavior is efficient and tailorable. The wavy heater follows the shape of a sinusoidal wave which is characterized by the spatial frequency along the longitudinal direction and the amplitude along the thickness direction, thus making its design parametrically defined. By exploiting the combination of these two design parameters, it is possible to achieve a higher electrical resistance of the heater for the same length of structure to be heated. Furthermore, the denser distribution of the heat source within the volume of the smart material also contributes to reducing the heating time. The heater is embedded into a smart material matrix composed of two identical 3D-printed sub-parts where the interface follows the shape of the wavy surface. To do so, laser-cut conductive tape is sandwiched between the two sub-parts and "glued" using UV curable resin [19]. We investigate the influences of the two design parameters. First, the influence on the arc length of the wavy heater in comparison with the flat heater is studied. Next, a numerical model is developed to calculate the heating time by varying the spatial frequency and amplitude of the wavy design [30]. The numerical results are compared and validated with experiments. A design map is given for predicting the heating durations within the design space. Finally, we demonstrate the stiffness tuning in thermoresponsive composite

* Corresponding author.
** Corresponding author.
E-mail addresses: zhangyuanfang@scut.edu.cn (Y.-F. Zhang), geq@sustech.edu.cn (Q. Ge).

https://doi.org/10.1016/j.coco.2023.101523
Received 29 November 2022; Received in revised form 24 January 2023; Accepted 1 February 2023
Available online 1 February 2023

structures with three-point bending tests. The proposed paradigm paves the way for the use of thermoresponsive smart materials on large-scale structures with applications in aerospace and architecture.

2. Materials and method

To fully exploit the spatial arrangement of heater within the smart material matrix, instead of embedding a flat heater, we propose the use of a 3D wavy heater in a sinusoidal form (Fig. 1a). The wavy heater is placed centered to the mid-plane of the matrix made of the thermoresponsive smart material. The two critical design parameters are the spatial frequency ν of the sinusoidal wave along the length direction of the structure and the amplitude A with regard to the mid-plane in the thickness direction. For the flat heater, the amplitude of the wave is zero. Meanwhile, for the wavy heater, the amplitude can vary from 0 to 1 when normalized with respect to the half-thickness of the structures.

While the length of the structure to be heated is the same, the normalized length λ of the wavy heater increases with both the amplitude A and the spatial frequency ν. By using the complete elliptic integral of the second kind, the relationship between λ and design parameters A, ν is given as follows:

$$\lambda = 1 + \nu \times \sum_{n=1}^{\infty} \left[\frac{(2n)!}{2^{2n} n!^2} \right]^2 \frac{\left(\sqrt{-1}A\right)^{2n}}{1-2n}, \tag{1}$$

where the right-hand side consists of two contributions, respectively the length of the flat heater and the additional arc length due to the waviness. While it is difficult to find a closed-form solution, approximate values of the wavy heater λ may be obtained numerically.

Fig. 1b shows the heat map of the theoretical wavy heater arc length as a function of these two design parameters. The range of the spatial frequency considered in this work is between 1 and 200. The arc length of the wavy heater is normalized with respect to the length of the flat heater. To facilitate visualization, the contours of the normalized length λ at respectively 1.5, 2.0, 2.5, 3.0, 3.5 and 4.0 are plotted. The heat map confirms that the heater arc length increases both with the spatial frequency and the amplitude. For combinations of large amplitude and large spatial frequency, the heater arc length may reach more than 4.0 times that of the flat heater.

To experimentally validate the design strategy, we fabricated bulky shape-memory polymer (SMP) rod structures with embedded flat and wavy Joule-heaters via a facile hybrid manufacturing approach, as depicted in Fig. 2. The heaters were prepared by laser-cutting conductive tapes into designed patterns. As the heater divides the SMP matrix into two sub-parts (Fig. 1a), the latter were first 3D-printed as separate parts with a commercial 3D printer, Polyjet J750 (Stratasys Ltd, Eden Prairie, MN, USA). The heater was then bonded to the interface between the two 3D-printed sub-parts.

Conductive fabrics or textiles have recently shown great potential as highly deformable and flexible heaters [31–36]. As illustrated in Fig. 2a, conductive silver fabric tapes were laser-cut into different lengths with mesh patterns which covered the arc length of the respective wavy design. The mesh patterns were used to provide a uniform flow of electrons in the heated area [37,38] and also to leave voids for the bonding of the SMP sub-parts. Fig. 2b displays each heater bonded to the interface of the respective 3D-printed sub-parts, namely for the flat design, the wavy design with a spatial frequency of 60 and an amplitude of 0.8 ($\nu = 60, A = 0.8$), and the wavy design with a spatial frequency of 120 and an amplitude of 0.8 ($\nu = 120, A = 0.8$). Fig. 2c demonstrates the assembled final prototype for the wavy design with a spatial frequency of 60 and an amplitude of 0.8 ($\nu = 60, A = 0.8$), where the two 3D-printed sub-parts were bonded together with UV curable resin via photopolymerization. The wavy heater was thus seamlessly integrated into the thermoresponsive smart material matrix.

3. Results and discussions

To help predict the heating performances with varying design parameters, we developed a numerical model based on a Green function formalism [39], in which design parameters such as the spatial frequency and the amplitude of the heater are robustly modifiable at reduced computational costs. Briefly, in this model, the transient heat transfer during the heating of SMP matrix with the wavy heater consists of three distinct contributions, namely the initial condition T_{IC}, the heat source T_{HS} and the boundary conditions T_{BC}, as depicted in Fig. 3a for the problem simplified to two dimensions (2D). The contributions are calculated separately by using a Green function matrix in a step-wise manner and then summed to yield the direct temperature solution:

$$T(x,y,t) = T_{IC} + T_{HS} + T_{BC}, \tag{2}$$

$$T_{IC} = F \int_{A'} G(x,y,t|x',y',0)\mathrm{d}A', \tag{3a}$$

$$T_{HS} = \frac{\alpha}{k} \int_{\tau=t'}^{t} \left[\int_{A'} g(x',y') G(x,y,t|x',y',\tau) dA' \right] \mathrm{d}\tau, \tag{3b}$$

$$T_{BC} = \frac{\alpha}{k} h T_{\infty} \int_{\tau=0}^{t} \left[\int_{\text{Boundary}} G(x,y,t|x',y',\tau)\mathrm{d}l' \right] \mathrm{d}\tau. \tag{3c}$$

where the Green function $G(x,y,t|x',y',\tau)$ describes the influence of the instantaneous energy released by a unit heat source on location (x',y') at time t perceived on any location (x,y) at time t greater than τ, F is the initial temperature field, α is the thermal diffusivity, k is the thermal conductivity, the function $g(x',y')$ describes the heat generated by the heating sources, h is the heat transfer coefficient, T_{∞} is a constant

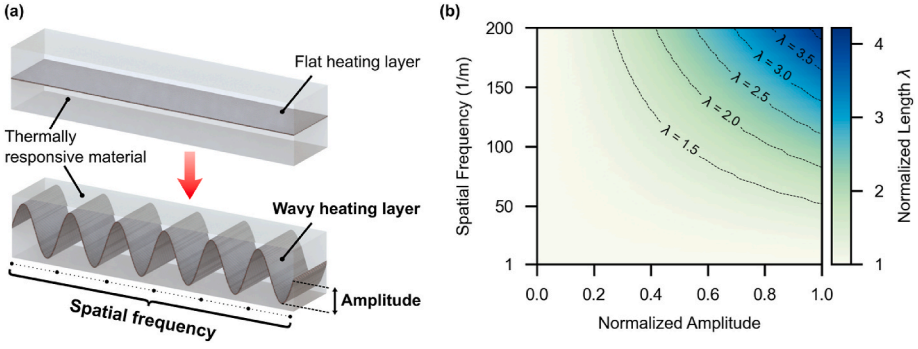

Fig. 1. Wavy design of embedded heater. (a) Parameters of wavy design. (b) Normalized heater length λ as a function of the spatial frequency and normalized amplitude.

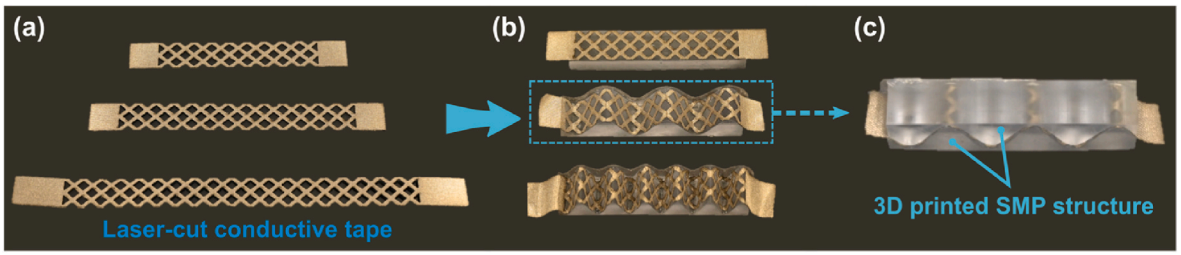

Fig. 2. Fabrication via a facile hybrid manufacturing approach of thick composite structures of SMP matrix embedded with flat or wavy Joule-heating layers. (a) Laser-cut conductive silver fabric tapes. (b) Bonding of the heaters to the interface of the respective 3D-printed sub-parts. (c) Assembled final prototype for the wavy design with a spatial frequency of 60 and an amplitude of 0.8.

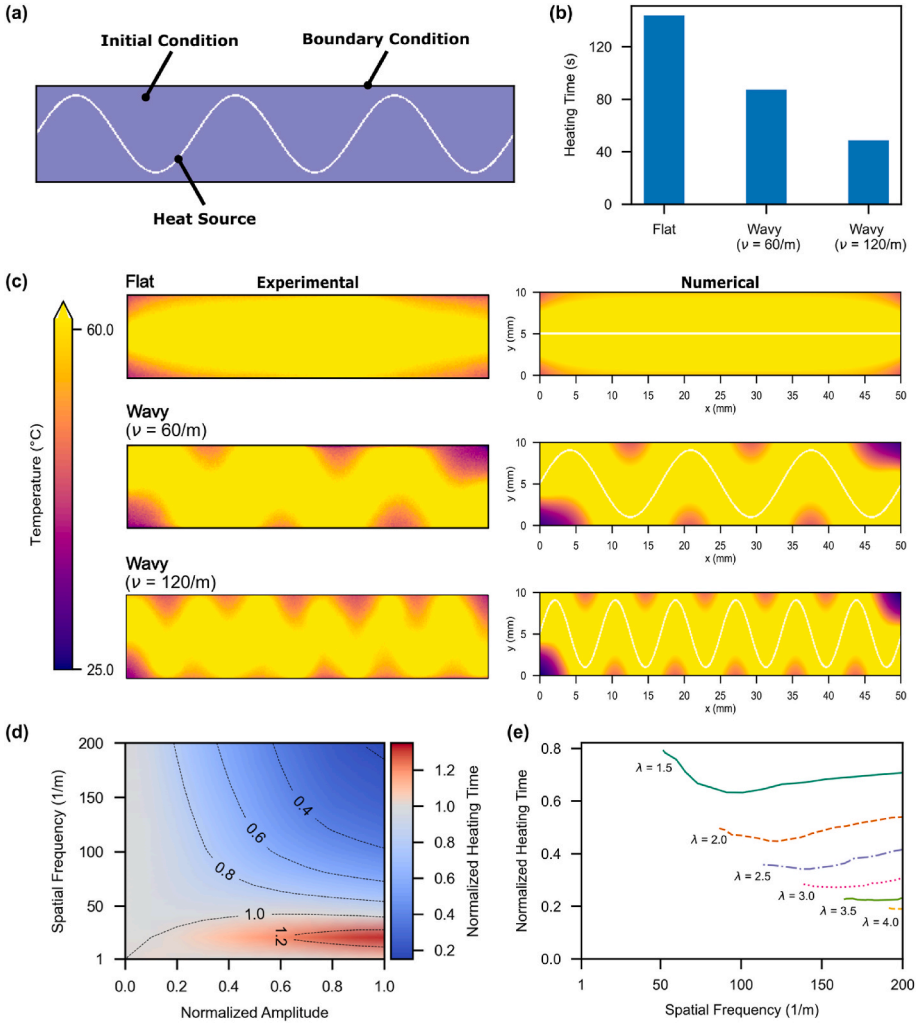

Fig. 3. A numerical model based on a Green function formalism for the prediction of the heating performances with varying design parameters. (a) Three distinct contributions to transient heat transfer during the heating of SMP matrix with the wavy heater. (b) Comparison of predicted minimum heating times for different designs of the heater. (c) Comparison of the experimental and numerical heat maps at the respective minimum heating times for three different heater designs, namely flat design, wavy design ($\nu = 60, A = 0.8$) and wavy design ($\nu = 120, A = 0.8$). (d) Design map for the prediction of normalized minimum heating time for different combinations of the spatial frequency and amplitude. (e) Variations of the minimum heating time with the spatial frequency at different total length levels. (For interpretation of the references to color in this figure legend, the reader is referred to the Web version of this article.)

ambient temperature, and t' denotes the instant when the heat source is powered on.

The evolution of the temperature field can thus be determined for different time steps. For the design of wavy heaters, we assume that the initial temperature field and the boundary conditions of convective nature are identical for all the designs. Therefore, the only varying parameter is the distribution of the heat source within the volume of the smart material matrix. This greatly simplifies the calculation, thus allowing multiple design scenarios to be computed and compared. More detailed explanation and validation of the numerical design framework can be found in our previous work [30].

For this numerical model, the actual distribution of the heat source and the heating power input could be determined parametrically from the sinusoidal wave equation. During the transient heat transfer, we could track the histogram of the temperature field and impose a design threshold. For example, in this work, we could define the minimum heating time as the time needed for 80% of the volume to surpass 60 °C which is the approximate value of the glass transition temperature of VeroClear (Stratasys Ltd, Eden Prairie, MN, USA), the smart material forming the matrix [17,19,30]. Fig. 3b shows the predicted minimum heating time of 144 s, 113 s and 57 s for respectively the flat design, the wavy design with a spatial frequency ν of 60 and an amplitude A of 0.8 ($\nu = 60, A = 0.8$), and the wavy design with a spatial frequency ν of 120 and amplitude A of 0.8 ($\nu = 120, A = 0.8$). In the numerical examples

presented in this work, the heat generated by the meshed heater is simplified as that generated by a uniform thin film heater of same total electrical resistance, estimated according to the measured resistance value per unit length (0.02 Ω/mm) and the theoretical arc length of each design. An input current of 2.0 A was used. The 2D cross-section of the SMP matrix has a length of 50 mm and a thickness of 10 mm. The SMP material has the following properties: the thermal conductivity is 0.238 W/m K^{-1}, the density is 1190 kg m^{-3}, and the average specific heat capacity is 2400 J/kg K^{-1} [19]. Compared with the flat design, the two wavy designs lead to an economy of heating time of respectively 22% (for $\nu = 60, A = 0.8$) and 60% (for $\nu = 120, A = 0.8$).

In Fig. 3c, we compare the experimental and numerical heat maps taken both at the respective minimum heating time for the three designs as presented in Fig. 3b. The experimental heat maps were recorded using an infrared thermal imaging camera InfReC R550-Pro (Nippon Avionics Co., Ltd., Japan). By using the same colorbar for the images, we observe a similar distribution of temperature across the 2D cross-section of the SMP matrix.

To further explore the design space, we calculated the minimum heating time for different combinations of spatial frequency and amplitude, as shown in Fig. 3d after normalization with respect to the minimum heating time with the flat heater design. To facilitate visualization, the contours for different levels of normalized heating time are plotted. For a small spatial frequency such as $\nu = 20$, the heating time could be even longer than that with the flat design, especially for larger amplitude where the heating is slow in the corners of the matrix that are distant from the peaks and valleys of the wavy shape. As the spatial frequency and amplitude increase, the heating time decreases significantly to as short as 0.18 times that with the flat design, in the case of wavy design with spatial frequency of 200 and amplitude of 1.0, corresponding to about 82% of economy in heating time.

While the parametric studies in Fig. 3d give the straightforward prediction that simultaneously increasing the spatial frequency and the amplitude helps reduce the heating time, it would be more interesting to explore how the spatial distribution of heat sources affects the heating time for a given heater length. We have therefore taken the contour lines for the heater length from Fig. 1b and projected them onto the design map in Fig. 3d to obtain variations of the minimum heating time with the spatial frequency at different total length levels (Fig. 3e). For each fixed total length, the feasible range of spatial frequency is bounded by a minimum value and the shortest heating time occurs at a spatial frequency slightly larger than the minimum value. As the total length increases, the minimum spatial frequency is shifted to the right, and the curve becomes flatter, thus rendering the difference in heating time between designs less pronounced. Fig. 3d and e provide insightful information for guiding the design of wavy heaters.

Thermoresponsive materials with stiffness that could be tunable over two or three orders of magnitudes find useful applications in fields like aerospace, architecture or robotics [16–22]. Tuning the stiffness of large-scale thermoresponsive composite structures in a controlled manner is highly desirable for practical purposes. To illustrate the stiffness tuning in thermoresponsive composite structures with the proposed strategy, we conducted three-point bending tests on three SMP rod structures incorporating different heater designs, and measured the force-displacement relationships under different thermal scenarios (Fig. 4). The tests were carried out on a universal mechanical testing machine, whose experimental setup is shown in Fig. 4a. The three heater designs presented in Fig. 2 were used. For each of the designs, three thermal scenarios were considered, namely at room temperature, heating for 30 s and heating for the minimum activation time shown in Fig. 3b.

The resulting force-displacement relationships are plotted in Fig. 4b. As the displacement increases, the curves become non-linear. We therefore calculated the bending stiffness values (Fig. 4c) by considering only the slopes of the linear part of the force-displacement curves. Despite slight discrepancies, the bending stiffness values remain around 200 kN/m for all three samples at room temperature, due to the high stiffness of the SMP in the glassy state. After heating the samples for 30 s, a sharp decrease in bending stiffness is observed, as the SMP material go into the rubbery state locally at high temperatures. The wavy design ($\nu = 120, A = 0.8$) shows the smallest bending stiffness among the three, and the flat design, the largest. This could be explained by the higher heating efficiency in the wavy designs. Finally, after heating the three samples for their respective minimum activation time, the bending stiffness values further decrease and tend to become similar.

Generally, the internal heating using embedded wavy heaters helps efficiently activate thermoresponsive composite structures, and eliminates the need of heating the surrounding environment which could be undesirable in many practical applications. While the proposed hybrid manufacturing scheme is easy to implement, direct additive manufacturing of thermoresponsive composite structures with embedded 3D heaters could be envisaged with further advances in 3D printing technologies of electronics.

4. Conclusions

In summary, this work presents a concept of embedding a wavy heater into a thermoresponsive material matrix to form a composite structure whose thermal activation behavior is efficient and tailorable. The arc length of the wavy heater, to which the electrical resistance of the heater is theoretically proportional, increases with both of the two design parameters, namely the amplitude and the spatial frequency, and can reach more than 4.0 times that of the flat heater. To further investigate the influence of the two design parameters, we developed a numerical model based on a Green function formalism to predict the transient heat transfer for varying wavy shapes of the heater. We experimentally validated the model on samples prepared with a hybrid fabrication approach. The evolution of the temperature field across the sample volume predicted by the model agrees well with the experiment. The exploration of the design space using the numerical model showed that the wavy design of heater could lead to an economy in heating time of as much as 82% in comparison with the flat design, thus making the thermal activation of the bulky composite structure much faster and more predictable. Finally, we demonstrated the stiffness tuning in

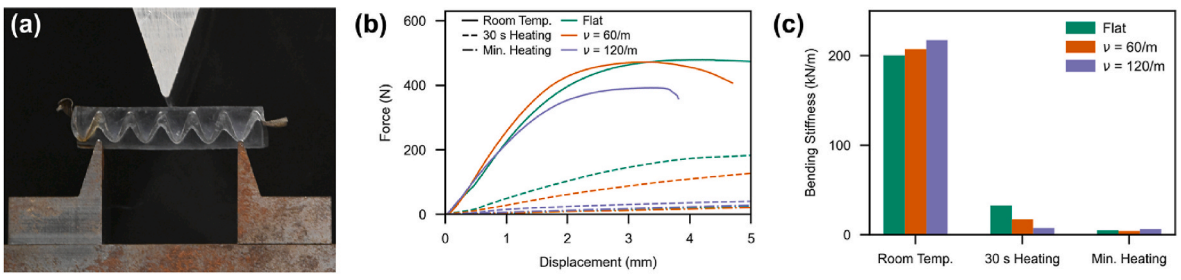

Fig. 4. Three-point bending test for three different heater designs under different thermal scenarios. (a) The experimental setup. (b) The force-displacement curves measured at midpoint. (c) The bending stiffness values characterized by the slopes of the linear part of the force-displacement curves.

thermoresponsive composite structures with three-point bending tests. The proposed paradigm could pave the way for the use of thermoresponsive smart materials on large-scale structures with applications in aerospace and architecture.

CRediT authorship contribution statement

Yuan-Fang Zhang: Conceptualization, Methodology, Writing – original draft, Writing – review & editing, Visualization, Supervision. **Honggeng Li:** Methodology, Validation, Investigation, Data curation, Visualization. **Chengyun Long:** Formal analysis, Writing – review & editing. **Yi Xiong:** Formal analysis, Writing – review & editing. **Qi Ge:** Writing – review & editing, Supervision.

Declaration of competing interest

The authors declare that they have no known competing financial interests or personal relationships that could have appeared to influence the work reported in this paper.

Data availability

Data will be made available on request.

Acknowledgements

Y.-F.Z. acknowledges the financial support from the Shien-Ming Wu School of Intelligent Engineering, South China University of Technology. Q.G. acknowledges the financial support from Korea Evaluation Institute of Industrial Technology (KEIT) for the research project of "The Development of PAD Printer System for Micro LED Multi-bonding Technology".

Appendix A. Supplementary data

Supplementary data to this article can be found online at https://doi.org/10.1016/j.coco.2023.101523.

References

[1] B.E. Schubert, D. Floreano, Variable stiffness material based on rigid low-melting-point-alloy microstructures embedded in soft poly(dimethylsiloxane) (PDMS), RSC Adv. 3 (2013) 24671–24679, https://doi.org/10.1039/c3ra44412k.
[2] W. Shan, T. Lu, C. Majidi, Soft-matter composites with electrically tunable elastic rigidity, Smart Mater. Struct. 22 (2013), 085005, https://doi.org/10.1088/0964-1726/22/8/085005.
[3] A. Miriyev, K. Stack, H. Lipson, Soft Material for Soft Actuators, Nat. Commun. 8 (2017) 596, https://doi.org/10.1038/s41467-017-00685-3.
[4] C. Yuan, D.J. Roach, C.K. Dunn, Q. Mu, X. Kuang, C.M. Yakacki, T.J. Wang, K. Yu, H.J. Qi, 3D printed reversible shape changing soft actuators assisted by liquid crystal elastomers, Soft Matter 13 (2017) 5558–5568, https://doi.org/10.1039/c7sm00759k.
[5] X. Xin, L. Liu, Y. Liu, J. Leng, Prediction of effective thermomechanical behavior of shape memory polymer composite with micro-damage interface, Compos. Commun. 25 (2021), 100727, https://doi.org/10.1016/j.coco.2021.100727.
[6] Y. Liu, W. Zhang, F. Zhang, X. Lan, J. Leng, S. Liu, X. Jia, C. Cotton, B. Sun, B. Gu, T.-W. Chou, Shape memory behavior and recovery force of 4D printed laminated miura-origami structures subjected to compressive loading, Compos. B Eng. 153 (2018) 233–242, https://doi.org/10.1016/j.compositesb.2018.07.053.
[7] L. Wang, Y. Yang, Y. Chen, C. Majidi, F. Iida, E. Askounis, Q. Pei, Controllable and reversible tuning of material rigidity for robot applications, materials, Today Off. 21 (2018) 563–576, https://doi.org/10.1016/j.mattod.2017.10.010.
[8] Z. Zhakypov, K. Mori, K. Hosoda, J. Paik, Designing minimal and scalable insect-inspired multi-locomotion millirobots, Nature 571 (2019) 381–386, https://doi.org/10.1038/s41586-019-1388-8.
[9] Z. Shen, F. Chen, X. Zhu, K.-T. Yong, G. Gu, Stimuli-responsive functional materials for soft robotics, J. Mater. Chem. B (2020), https://doi.org/10.1039/d0tb01585g.
[10] Y. Wang, Z. Wang, Q. He, P. Iyer, S. Cai, Electrically controlled soft actuators with multiple and reprogrammable actuation modes, Adv. Intell. Syst. 2 (2020), 1900177, https://doi.org/10.1002/aisy.201900177.
[11] F. Qin, H.-Y. Cheng, R. Sneeringer, M. Vlachostergiou, S. Acharya, H. Liu, C. Majidi, M. Islam, L. Yao, ExoForm: shape memory and self-fusing semi-rigid wearables, in: Extended Abstracts of the 2021 CHI Conference on Human Factors in Computing Systems, ACM, Yokohama Japan, 2021, pp. 1–8, https://doi.org/10.1145/3411763.3451818.
[12] Z. Xing, F. Wang, Y. Ji, D. McCoul, X. Wang, J. Zhao, A structure for fast stiffness-variation and omnidirectional-steering continuum manipulator, IEEE Rob. Autom. Lett. 6 (2021) 755–762, https://doi.org/10.1109/lra.2020.3037858.
[13] K. Zhang, H. Lv, Y. Zheng, Y. Yao, X. Li, J. Yu, B. Ding, Nanofibrous hydrogels embedded with phase-change materials: temperature-responsive dressings for accelerating skin wound healing, Compos. Commun. 25 (2021), 100752, https://doi.org/10.1016/j.coco.2021.100752.
[14] Y.-F. Zhang, Z. Li, H. Li, H. Li, Y. Xiong, X. Zhu, H. Lan, Q. Ge, Fractal-based stretchable circuits via electric-field-driven microscale 3D printing for localized heating of shape memory polymers in 4D printing, ACS Appl. Mater. Interfaces (2021), https://doi.org/10.1021/acsami.1c03572.
[15] S. Lee, Y. Kim, D. Park, J. Kim, The thermal properties of a UV curable acrylate composite prepared by digital light processing 3d printing, Compos. Commun. 26 (2021), 100796, https://doi.org/10.1016/j.coco.2021.100796.
[16] T.L. Buckner, E.L. White, M.C. Yuen, R.A. Bilodeau, R.K. Kramer, A move-and-hold pneumatic actuator enabled by self-softening variable stiffness materials, in: 2017 IEEE/RSJ International Conference on Intelligent Robots and Systems, IROS, 2017, pp. 3728–3733, https://doi.org/10.1109/iros.2017.8206221.
[17] S. Akbari, A.H. Sakhaei, K. Kowsari, B. Yang, A. Serjouei, Y.-F. Zhang, Q. Ge, Enhanced multimaterial 4D printing with active hinges, Smart Mater. Struct. 27 (2018), 065027, https://doi.org/10.1088/1361-665x/aabe63.
[18] Y. Hao, T. Wang, Z. Xie, W. Sun, Z. Liu, X. Fang, M. Yang, L. Wen, A eutectic-alloy-infused soft actuator with sensing, tunable degrees of freedom, and stiffness properties, J. Micromech. Microeng. 28 (2018), 024004, https://doi.org/10.1088/1361-6439/aa9d0e.
[19] Y.-F. Zhang, N. Zhang, H. Hingorani, N. Ding, D. Wang, C. Yuan, B. Zhang, G. Gu, Q. Ge, Stiffness-tunable soft actuator by hybrid multimaterial 3D printing, Fast-Response, Adv. Funct. Mater. 29 (2019), 1806698, https://doi.org/10.1002/adfm.201806698.
[20] T.L. Buckner, M.C. Yuen, S.Y. Kim, R. Kramer-Bottiglio, Enhanced variable stiffness and variable stretchability enabled by phase-changing particulate additives, Adv. Funct. Mater. 29 (2019), 1903368, https://doi.org/10.1002/adfm.201903368.
[21] Y. Yu, H. Liu, K. Qian, H. Yang, M. McGehee, J. Gu, D. Luo, L. Yao, Y.J. Zhang, Material characterization and precise finite element analysis of fiber reinforced thermoplastic composites for 4D printing, Comput. Aided Des. 122 (2020), 102817, https://doi.org/10.1016/j.cad.2020.102817.
[22] B. Zhang, H. Li, J. Cheng, H. Ye, A.H. Sakhaei, C. Yuan, P. Rao, Y.-F. Zhang, Z. Chen, R. Wang, X. He, J. Liu, R. Xiao, S. Qu, Q. Ge, Mechanically Robust and UV-Curable Shape-Memory Polymers for Digital Light Processing Based 4D Printing, Advanced Materials, n/a, 2021, 2101298, https://doi.org/10.1002/adma.202101298.
[23] J.E.M. Teoh, Y. Zhao, J. An, C.K. Chua, Y. Liu, Multi-stage responsive 4D printed smart structure through varying geometric thickness of shape memory polymer, Smart Mater. Struct. 26 (2017), 125001, https://doi.org/10.1088/1361-665x/aa908a.
[24] W.L. Shan, T. Lu, Z.H. Wang, C. Majidi, Thermal analysis and design of a multi-layered rigidity tunable composite, Int. J. Heat Mass Tran. 66 (2013) 271–278, https://doi.org/10.1016/j.ijheatmasstransfer.2013.07.031.
[25] Y. Li, N.C. Goulbourne, Numerical simulations for microvascular shape memory polymer composites, Smart Mater. Struct. 24 (2015), 055022, https://doi.org/10.1088/0964-1726/24/5/055022.
[26] Q. Mu, L. Wang, C.K. Dunn, X. Kuang, F. Duan, Z. Zhang, H.J. Qi, T. Wang, Digital light processing 3D printing of conductive complex structures, Addit. Manuf. 18 (2017) 74–83, https://doi.org/10.1016/j.addma.2017.08.011.
[27] A. Zolfagharian, A. Kaynak, S.Y. Khoo, A. Kouzani, Pattern-driven 4D printing, Sensor Actuator Phys. 274 (2018) 231–243, https://doi.org/10.1016/j.sna.2018.03.034.
[28] Y. Yin, M. Li, W. Yuan, X. Chen, Y. Li, A widely adaptable analytical method for thermal analysis of flexible electronics with complex heat source structures, Proc. R. Soc. A. 475 (2019), 20190402, https://doi.org/10.1098/rspa.2019.0402.
[29] X. Huang, F. Zhang, J. Leng, Metal mesh embedded in colorless shape memory polyimide for flexible transparent electric-heater and actuators, Appl. Mater. Today 21 (2020), 100797, https://doi.org/10.1016/j.apmt.2020.100797.
[30] Y.-F. Zhang, Q. Ge, A numerical framework for the design of joule-heating circuits to thermally activate smart materials, Smart Mater. Struct. 28 (2019), 115026, https://doi.org/10.1088/1361-665x/ab47e4.
[31] Y. Li, Z. Zhang, X. Li, J. Zhang, H. Lou, X. Shi, X. Cheng, H. Peng, A smart, stretchable resistive heater textile, J. Mater. Chem. C 5 (2016) 41–46, https://doi.org/10.1039/c6tc04399b.
[32] T.L. Buckner, R. Kramer-Bottiglio, Functional fibers for robotic fabrics, Multifunct. Mater. 1 (2018), 012001, https://doi.org/10.1088/2399-7532/aad378.
[33] M. Cartolano, B. Xia, A. Miriyev, H. Lipson, Conductive fabric heaters for heat-activated soft actuators, Actuators 8 (2019) 9, https://doi.org/10.3390/act8010009.
[34] V. Sanchez, C.J. Payne, D.J. Preston, J.T. Alvarez, J.C. Weaver, A.T. Atalay, M. Boyvat, D.M. Vogt, R.J. Wood, G.M. Whitesides, C.J. Walsh, Smart Thermally Actuating Textiles, Advanced Materials Technologies, n/a, 2020, 2000383, https://doi.org/10.1002/admt.202000383.
[35] X. Zhang, X. Chao, L. Lou, J. Fan, Q. Chen, B. Li, L. Ye, D. Shou, Personal thermal management by thermally conductive composites: a review, Compos. Commun. 23 (2021), 100595, https://doi.org/10.1016/j.coco.2020.100595.
[36] V. Sanchez, C.J. Walsh, R.J. Wood, Textile Technology for Soft Robotic and Autonomous Garments, Advanced Functional Materials, n/a, 2021, 2008278, https://doi.org/10.1002/adfm.202008278.

[37] X. Zhu, Q. Xu, H. Li, M. Liu, Z. Li, K. Yang, J. Zhao, L. Qian, Z. Peng, G. Zhang, J. Yang, F. Wang, D. Li, H. Lan, Fabrication of high-performance silver mesh for transparent glass heaters via electric-field-driven microscale 3D printing and UV-assisted microtransfer, Adv. Mater. 31 (2019), 1902479, https://doi.org/10.1002/adma.201902479.

[38] X. Zhu, M. Liu, X. Qi, H. Li, Y.-F. Zhang, Z. Li, Z. Peng, J. Yang, L. Qian, Q. Xu, N. Gou, J. He, D. Li, H. Lan, Templateless, plating-free fabrication of flexible transparent electrodes with embedded silver mesh by electric-field-driven microscale 3D printing and hybrid hot embossing, Adv. Mater. 33 (2021), 2007772, https://doi.org/10.1002/adma.202007772.

[39] W.J. Mansur, C.A.B. Vasconcellos, N.J.M. Zambrozuski, O.C. Rotunno Filho, Numerical solution for the linear transient heat conduction equation using an explicit Green's approach, Int. J. Heat Mass Tran. 52 (2009) 694–701, https://doi.org/10.1016/j.ijheatmasstransfer.2008.07.036.